Bipolar Electrochemical Mechanism for Mass Transfer in Nanoionic Resistive Memories

Xuezeng Tian, Shize Yang, Min Zeng, Lifen Wang, Jiake Wei, Zhi Xu,* Wenlong Wang, and Xuedong Bai*

Solid-electrolyte-based nanoionic resistive memories (ReRAM), also known as electrochemical metallization memories (ECM), are electrically driven switching devices that can retain an internal resistance based on the history of applied voltage and current. These ReRAMs are considered to be promising candidates as next-generation, non-volatile memory devices thanks to their high endurance, fast switching time, and outstanding scaling capability.[1–5] Research efforts are now focused on a microscopic understanding of the physicochemical processes responsible for resistive switching and on novel applications including reconfigurable logic systems and neuromorphic computing.[6–10] Generally, a nanoscale conductive filament model is adopted for the microscopic switching mechanism. This model is based on the electrochemical dissolution and deposition of active electrode metals (such as Ag or Cu) in the solid electrolyte layer, which generally leads to the formation of conductive filaments, hence they were termed electrochemical metallization memories.[5,11] Although these conductive filaments have been visualized in many works, the physicochemical processes at the nanoscale are still controversial.[12–18] The observed morphologies of the conductive filaments were highly different according to different reports.[12,14,16] Those differences are closely related to the filament formation process, which as yet has not been properly clarified. Details of the dynamic processes were mainly limited by the experimental setup or the type of sample in previous reports.

In this work, deliberately designed ECM devices have been investigated using an in-situ transmission electron microscope (TEM). It is demonstrated that the formation and disruption of the conducting filament is driven by the bipolar electrochemical mass transfer of Ag in the solid SiO_2 electrolyte. The novel sample structure and the atomic-scale images have provided us with unambiguous details of the mass-transfer processes. Based on the high-resolution observations the detailed redox reaction dynamics are clarified.

The two sample structures used in this work were designed for different purposes. One design consists of a $Ag/SiO_2/Si$ sandwich structure for reproducing the real devices inside the TEM. The other is composed of a silver-embedded SiO_2 structure, which was dedicatedly designed to disclose the

X. Tian, S. Yang, M. Zeng, L. Wang, J. Wei, Dr. Z. Xu,
Prof. W. Wang, Prof. X. Bai
Beijing National Laboratory
for Condensed Matter Physics
Institute of Physics
Chinese Academy of Sciences
Beijing 100190, China
E-mail: xuzhi@iphy.ac.cn; xdbai@iphy.ac.cn

driving force for the electrochemical reactions. For the first structure, we firstly tested the switching performance of the devices outside the TEM column (setups shown in **Figure 1**a, top panel). Then we conducted the in-situ TEM experiments thereby reproducing the performance of the ex-situ devices; a Ag tip driven by a nanomanipulator was used as the active metal electrode (Figure 1a, bottom panel). To switch the pristine insulating device to its conductive state, a constant bias of 8V was applied to the silver tip with an appropriate current compliance. The current versus time curve is shown in Figure 1b. Serial images corresponding to the numbered arrows of Figure 1b are shown in Figure 1c. The current curves and the images were recorded simultaneously.

After applying the voltage stress for 34 s, a cluster appeared near the anodic Ag tip. Subsequently a series of new clusters grew up towards the Si electrode right next to the first cluster. After applying the voltage for 62 s, the current increased abruptly (arrow 5 in Figure 1b), corresponding to the conductive filament reaching the bottom electrode. These clusters are found to be composed of pure Ag from high-resolution images and energy-dispersive X-ray spectroscopy (Figure S1 and S2, Supporting Information). From these real-time images, four features can be noticed. Firstly, the conductive channel grows from the anode to the cathode in a step-by-step manner. Secondly, it is rather a series of clusters than a continuous filament that bridges the two electrodes. Thirdly, after the current reaches compliance, in other words, when the filament reaches the bottom electrode, the mass transfer of silver continues, with more silver clusters growing, as can be seen in images 5 and 6 of Figure 1c. And the fourth remark that can be made is that new clusters grow faster as they approach the bottom electrode (Supplementary Video S1, Supporting Information). The cluster-after-cluster growth mode is highly indicative of the mass-transfer dynamics and will be addressed later.

Then, the device was switched off by applying a reverse bias of –6 V. The erasing process was extremely fast. As soon as the conducting channel breaks near the bottom electrode, an abrupt current drop occurs (Parts 1 and 2 of Figure 1e). This evidence verifies the former hypothesis on ECM cells that filaments break close to the bottom electrode when switched off.[19–21] Further applying of the reversed bias made additional clusters disappear. The continuing growth of clusters after switch on and shrinking of clusters after switch off are novel phenomena to be noticed.

In contrast to the original ECM theory, which predicts a cathode to anode filament growth, our observation has shown an opposite growth mode from the anode to the cathode. A similar phenomenon was reported elsewhere.[16] In the former publication, this phenomenon was explained by the
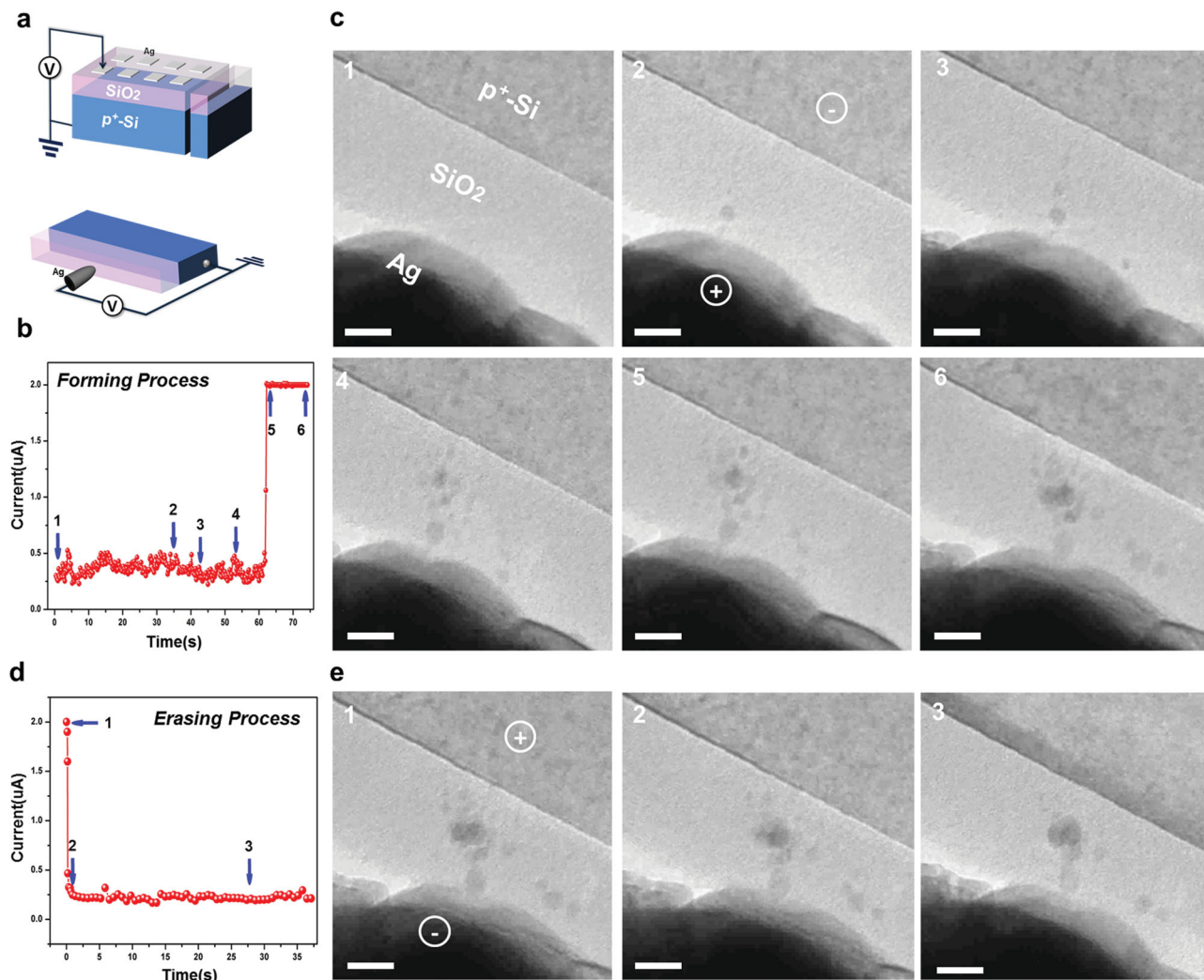
Figure 1. Experimental setup and dynamic electrochemical mass transfer process. a) Schematic of ex-situ (top panel) and in-situ (bottom panel) experimental setup. b) I–t characteristics recorded during the switching process at a voltage of 8 V. c) TEM images corresponding to data points 1–6 in (b). The six images were extracted from a video (see supplementary Video S1, Supporting Information) recorded during the switching process. Scale bar is 10 nm. d) I–t characteristics recorded during the reversed voltage stress of –6 V. e) TEM images corresponding to data points 1–3 in (d). Scale bar is 10 nm.

overwhelming quantity of electrons in the electrolyte that reduce the silver ions. A key question here is how can the silver atoms be anodized from the clusters and move forwards if the clusters are surrounded by an ocean of electrons.

To better understand the dynamics of the mass transfer of silver in SiO_2, we designed a second sample structure by embedding silver clusters in the middle of a SiO_2 matrix, as **Figure 2**a shows (see details in Experimental Section). The embedded silver clusters are in the cubic phase, as shown in Figure 2c. In this sample, the silver clusters are isolated from both the anode and the cathode, and, thus, can be regarded as bipolar electrodes (BPEs). The mechanism of a BPE is based on the polarization of a conductive object exposed to an external electric field, as shown in Figure 2b. As the conductive object is an equipotential body, the local potential profile will be changed and the object becomes polarized.[22,23] The resulting polarization $\Delta\phi_\theta$ at the cluster surface (r,θ) is given by

$$\Delta\phi_\theta = E \cdot r \left(\cos\theta - \cos\lambda \right) \qquad (1)$$

where E is the electric field, r is the radius of the particle, and λ defines the position where $\Delta\phi_\theta = 0$. When the polarization is high enough, the anodic reaction will occur at the surface. Interestingly, compared to former experiments and predictions, our in-situ experiments show a quite different growth behavior.[24,25] The major difference with former reports lies in our choice of electrolyte materials, that is, we used SiO_2 instead of a silver ion conductor. For silver ion conductors, silver ions would only be reduced at the interface of the electrolyte and the cathode, whereas in our experiment, the silver ions were readily reduced within the SiO_2 matrix.

The experimental setup was the same as in Figure 1a, except that the tip was Au. By applying a sufficient positive or negative voltage to the Au tip, the buried clusters were polarized by the established electric field and electrochemical reactions
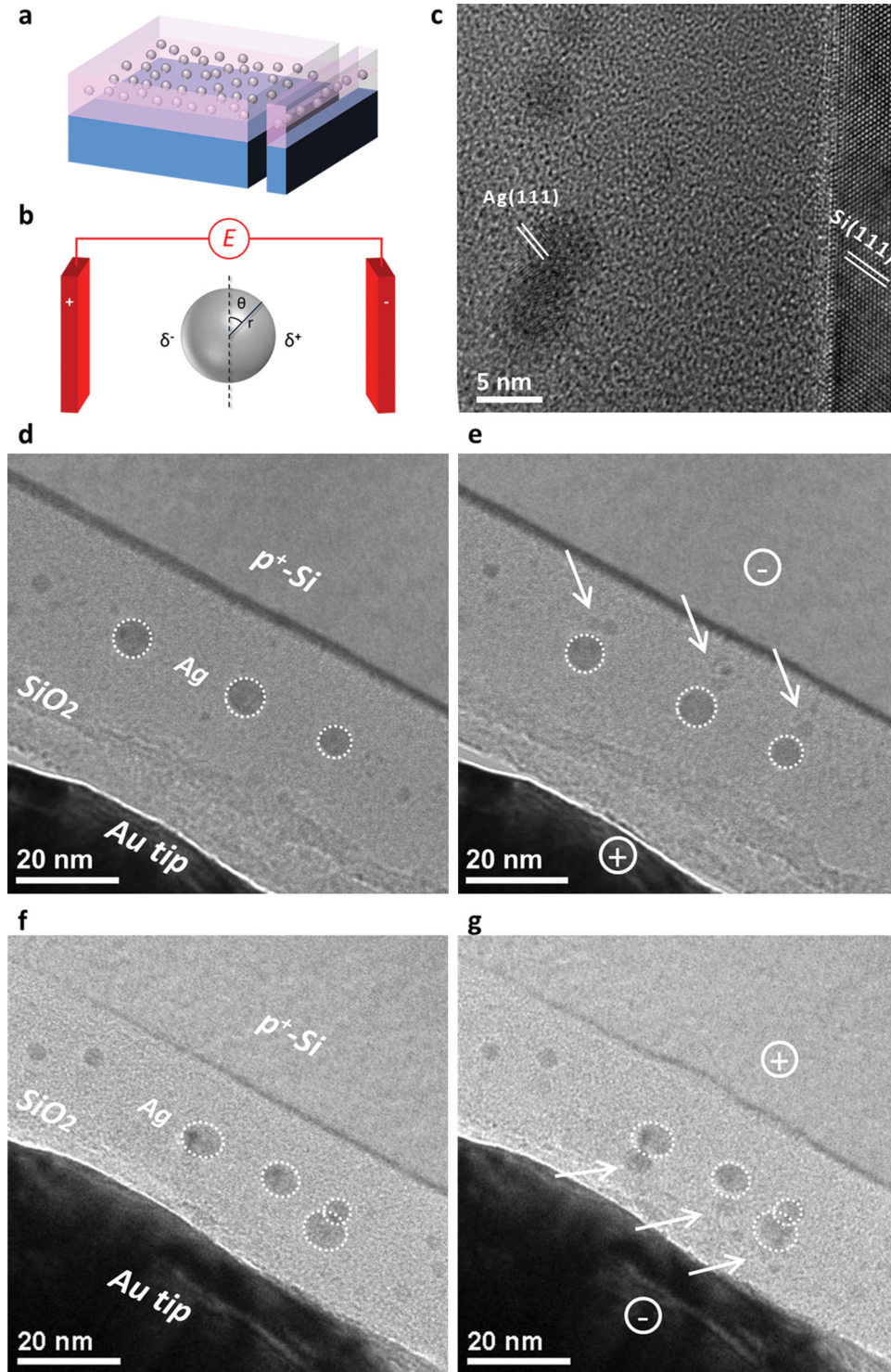
Figure 2. Mass transfer based on bipolar electrochemistry within a silver-embedded sample. a) Schematic of the sample structure with embedded Ag clusters. b) Schematic of the bipolar electrode. c) TEM image of the freshly made sample. The lattice fringes are indexed to *fcc* silver (111). d,f) Images of the sample prior to the in-situ experiment. e,g) Images of the sample after the in-situ experiments corresponding to images (d) and (f), respectively. The applied voltages in (e) and (g) were opposite to each other, as labeled by the + and − signs. The arrows indicate the emerging of new silver clusters from the original ones in consistent with the directions of the electric field.

were triggered. From Figure 2e and Figure 2g, we can see that the growth direction of the buried silver clusters complies with the direction of the electric field. New clusters were formed adjacent to the original clusters, as indicated by the arrows. This observation also verifies that the Ag cluster growth is not caused by the electron-beam irradiation.
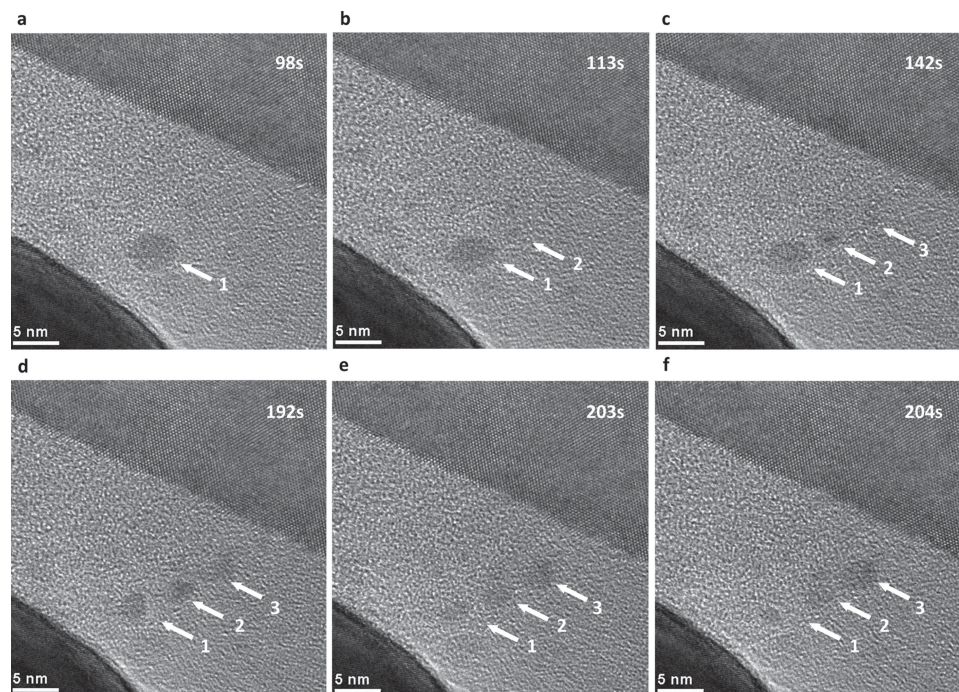
Figure 3. Serial images of high-resolution mass-transfer process in the silver-embedded sample. a–f) Images of the mass-transfer process at the stressing time of 98s, 113 s, 142 s, 192 s, 203 s, and 204 s, respectively. The images were extracted from a real-time recorded video. Arrow 1 indicates the original cluster. Arrows 2 and 3 indicate the first and second new-born clusters, respectively. The stressing voltage was 8 V.

Using this structural model, we were able to study the silver mass-transfer process more clearly. A series of high-resolution captures of the mass transfer of the Ag clusters is shown in **Figure 3** (see Supplementary Video S2, Supporting Information). New clusters appeared and grew nearby the original clusters. Note that there was always a nanogap between the neighboring clusters. As the reaction proceeded, the original cluster (cluster 1) was slowly consumed to be smaller and smaller, and the new clusters (cluster 2 and 3) grew bigger. As a net effect, the Ag cluster group moved forward along the electric field direction.

By carefully studying the mass-transfer process in Figure 3, we have been able to explain how the new clusters appeared in the electrolyte and how re-oxidation took place on those clusters. The key is that the role of cluster 2 changes with the mass-transfer process. At the beginning, cluster 2 appears due to the cathodic reduction and nucleation of silver ions from cluster 1. It, thus, acts as the cathode to cluster 1. The redox couple is then cluster 1 – cluster 2. No anodic reaction takes place on cluster 2 at this stage. But as cluster 2 grows larger, it changes the local equipotential. According to Equation (1), when the size of cluster 2 exceeds a certain value, the polarization induced by the external electric field will be adequate to oxidize the silver atoms at the anodic pole. This stage corresponds to the emerging of cluster 3, as shown in Figure 3c. Thus a new redox couple is formed by cluster 2 and cluster 3. At this stage, both a reduction reaction and oxidation reaction occur on cluster 2. It behaves as a BPE. From Figure 3d to Figure 3f, it is interesting to notice that the size of cluster 2 remains almost the same. During this process, it seems that cluster 2 functions as a transit station. This indicates that the

rate of the reduction reaction is comparable to that of the oxidation reaction. Gradually cluster 1 is consumed and cluster 3 grows bigger and bigger.

We believe that the change in role of the newborn clusters is essential in the mass transfer of silver in the SiO$_2$ matrix, which is consistent with the results shown in Figure 1c. Firstly a new cluster was born adjacent to the silver source. As it grew larger, another new cluster would be born from it. But the first cluster remained almost unchanged even though the subsequent clusters all originated from it. The first cluster thus acted as the BPE. The difference with the silver-embedded sample was that the silver tip acted as an infinite silver source, thus the formed silver clusters wouldn't be consumed as the mass transfer continued. By repeating this process, a series of silver clusters were formed until finally bridging the electrodes.

We also analyzed the above phenomena from the viewpoint of electrochemical potentials. For bipolar electrochemistry, it has to be noted that the interfacial potential difference between the electrode and the electrolyte, rather than the absolute potential of either, is the driving force for electron transfer.[26] In our case, the electrical potential is applied to a metal/insulator/metal (MIM)-type cell with a metal ion (Ag$^+$)-electron mixed conducting electrolyte (SiO$_2$). The electrochemical potential of the electrons ($\tilde{\mu}_e$) in the electrolyte, which is identical to the Fermi level E_F, can be expressed as follows:

$$\tilde{\mu}_e = \mu_e - F\phi = \left(\mu_{e^0} + RT \ln n_e\right) - F\phi \tag{2}$$

where μ_e is the chemical potential of the electrons, F is the Faraday constant, ϕ is the internal potential (the electrostatic potential with reference to infinity), μ_e^0 is the standard chemical

potential of electrons in equilibrium with the reference silver activity of unity, and n_e is the electron density per unit volume. Assuming a uniform electrolyte layer and no electronic overvoltage at the interfaces (e.g., Schottky barriers), both $\tilde{\mu}_e$ and ϕ should have approximately linear profiles.[22] The silver cluster will change the local equipotential and become polarized. The schematics in **Figure 4**a and 4b correspond to Figure 3b and 3c, respectively. When a sufficient voltage is applied, the silver atoms at the anodic pole will be oxidized into silver ions within the SiO$_2$ matrix. After they have drifted over a small distance (from x_2 to x_3), they are reduced by the local electrons, where $E_F(x_3)$-$E_F(x_2)$ > $E_F(Ag/Ag^+)$, and nucleate into a cluster. When the size of the new cluster exceeds a certain value, the anodic polarization will be sufficient to give rise to oxidizing reactions. At this stage, the newly born cluster acts as a BPE. Thus the mass transfer can proceed. The real energy diagram is more complicated, as in our analysis we have ignored both the electronic overvoltage at the interfaces and the influence of ionic conduction on the potential distribution. The coupling of the electronic and ionic properties is also simplified. These underestimated factors could be very influential in the device performance and offer potential for further device innovation and optimization.[27–29]

Based on the above discussion, a reasonable supposition can be made, namely, that there is a critical size of the clusters for a given situation, beyond which the polarization is strong enough to provide the electromotive force for bipolar reactions. The critical size in Figure 1c is about 5 nm under an electric field of 0.25 V nm^{-1}. In Figure 3c it is about 3 nm under an electric field of 0.4 V nm^{-1}. The potential difference between the two ends of the BPE is around 1.2 eV. This value is comparable to the solution-based standard redox potential of silver.[30] However, the critical size is not universal because the real situation is more complicated as the electrochemical reaction is also influenced by many other factors, such as the pressure,

temperature, local infrastructure, and especially the redistribution of the potential profile with the growth of the clusters in the electrolyte. We have also simulated the electric-field distribution and the potential profile for different sizes of bipolar electrodes using a finite element method (see Figure S3, Supporting Information). The simulated results verify the potential change and electric-field redistribution induced by those BPEs with different sizes. The polarizations were found to be highly dependent on the cluster size.

The mass-transfer behavior of the embedded clusters are in accordance with the case in Figure 1, except that the silver sources are different. The same BPE mass-transfer mode can be applied to the first sample structure. A Fermi-level diagram for the first sample is shown in Figure S4 in the Supporting Information. Based on the bipolar electrochemical mechanism, all the growth features disclosed in Figure 1 can be well addressed. The filament grows faster and faster, because the potential slope becomes larger and larger. When the filament comes to reach the cathode and the current becomes compliant, the potential differences between the neighboring clusters are still big enough to give rise to electrochemical reactions. So the mass transfer continues, making the filament more robust. This implies that the mass transfer will not terminate until the potential difference is really small. The continuing growth of these conductive filaments may deteriorate the nanogaps between neighboring clusters, which may lead to the device degradation.

In summary, we have provided detailed dynamic processes of the mass-transfer process of Ag in solid SiO$_2$ using an in-situ observation method. The step-by-step mass transfer supports a bipolar electrochemical mechanism for the conductive filament formation. Based on the observations and Fermi-level analysis, the mass-transfer dynamics were clarified. This work could provide the basis for establishing a reliable physical picture of device operation and could help to guide research into further
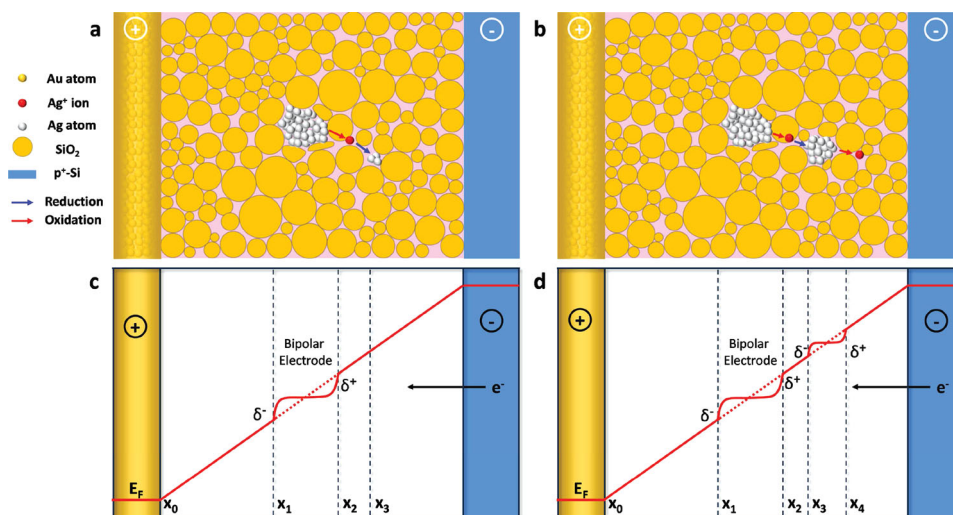
Figure 4. Schematic pictures and Fermi level diagrams for different mass-transfer stages. a) Schematic showing the first new cluster emerging, corresponding to Figure 3b. At this stage, only cathodic reaction takes place on the emerging cluster. b) Schematic showing the second new cluster emerging from the first one. At this stage, both cathodic and anodic reactions take place on the first cluster. c) Schematic Fermi-level diagram corresponding to (a). d) Schematic Fermi-level diagram corresponding to (b). Note that the electrochemical potential of the electrons $\tilde{\mu}_e$ in the electrolyte is identical to the Fermi level E_F.

COMMUNICATION

device optimization. We emphasize that the choice of electrolyte material highly influences the mass-transfer mechanism. We also call attention to the fact that the cluster-forming operation should be carefully conducted and over-forming should be avoided as it may lead to device degradation.

Experimental Section

Sample preparation: The substrates for film deposition were heavily doped p-type silicon purchased from MTI Corporation, with a resistivity of 10^{-2} Ω cm^{-1}. The SiO_2 films were deposited by plasma-enhanced chemical vapor deposition (PECVD) at a temperature of 180 °C, using dinitrogen oxide and silane as the precursors. Silver and gold tips for in-situ measurements were made using a homemade electrochemical corrosion cell using 1 M KOH solution electrolyte. The tips were typically 30 nm at the sharpest end. The silver-embedded structure was made by depositing 20 nm SiO_2, 0.5 nm silver, 20 nm SiO_2 onto the substrate in sequence. The evaporated silver occurred naturally in a spherical shape, as shown in Figure 2b. All the cross-section TEM samples were made by traditional manual grinding and milling by an RES 101 ion miller to achieve a clean surface. We estimated the thickness of the interesting areas of the samples to be about 30 nm to 60 nm, using electron energy loss spectroscopy (EELS) analyzed by Digital Micrograph software.

Device measurements: For all measurements, the silicon substrate was ground and a compliance current was applied to protect the devices. The ex-situ measurements were carried out using a semiconductor analyzer Agilent B1500 at ambient environmental conditions. The in-situ measurements were conducted in a JEOL 2010F TEM combined with an Agilent B2900 Precision Source/Measure Unit (SMU). An accelerating voltage of 200 kV was used. The TEM holders in our experiments were all homemade and dedicatedly designed for in-situ TEM experiments. The silver or gold tip was driven by a nanomanipulator as a movable top electrode.

It has been noted before that the electron beam has a softening effect on SiO_2, and that electron-beam irradiation can cause Ag diffusion, according to the literature.[31,32] We compared different electron-beam illuminating conditions including shutting off the illumination, and found that the morphologies of the filaments were consistent (see the control experiment results in Figure S5, Supporting Information). During the experiment, the brightness of the electron beam was reduced to the minimum requirement for photographing in order to reduce the actual influence of the electron beam.

Computer simulation: We applied a finite element method to create the computer simulation. The parameters are specified in Figure S3 in the Supporting Information.

Supporting Information

Supporting Information is available from the Wiley Online Library or from the author.

Acknowledgements

[1] I. Valov, R. Waser, J. R. Jameson, M. N. Kozicki, *Nanotechnology* **2011**, *22*, 289 502.

[2] W. Lu, D. S. Jeong, M. Kozicki, R. Waser, *MRS Bull.* **2012**, *37*, 124.

[3] J. J. S. Yang, D. B. Strukov, D. R. Stewart, *Nat. Nanotechnol.* **2013**, *8*, 13.

[4] Y. Fujisaki, *Jpn. J. Appl. Phys.* **2013**, *52*, 040 001.

[5] R. Waser, R. Dittmann, G. Staikov, K. Szot, *Adv. Mater.* **2009**, *21*, 2632.

[6] D. H. Kwon, K. M. Kim, J. H. Jang, J. M. Jeon, M. H. Lee, G. H. Kim, X. S. Li, G. S. Park, B. Lee, S. Han, M. Kim, C. S. Hwang, *Nat. Nanotechnol.* **2010**, *5*, 148.

[7] J. Borghetti, G. S. Snider, P. J. Kuekes, J. J. Yang, D. R. Stewart, R. S. Williams, *Nature* **2010**, *464*, 873.

[8] S. Tanachutiwat, M. Liu, W. Wang, *IEEE Trans. Very Large Scale Integr. VLSI Syst.* **2011**, *19*, 2023.

[9] T. Chang, S. Jo, W. Lu, *ACS Nano* **2011**, *5*, 7669.

[10] D. Seok Jeong, I. Kim, M. Ziegler, H. Kohlstedt, *RSC Advances* **2013**, *3*, 3169.

[11] R. Waser, M. Aono, *Nat. Mater.* **2007**, *6*, 833.

[12] X. Guo, C. Schindler, S. Menzel, R. Waser, *Appl. Phys. Lett.* **2007**, *91*, 133 513.

[13] B. Cho, J. Yun, S. Song, Y. Ji, D. Kim, T. Lee, *Adv. Funct. Mater.* **2011**, *21*, 3976.

[14] Q. Liu, J. Sun, H. Lv, S. Long, K. Yin, N. Wan, Y. Li, L. Sun, M. Liu, *Adv. Mater.* **2012**, *24*, 1844.

[15] I. Valov, I. Sapezanskaia, A. Nayak, T. Tsuruoka, T. Bredow, T. Hasegawa, G. Staikov, M. Aono, R. Waser, *Nat. Mater.* **2012**, *11*, 530.

[16] Y. Yang, P. Gao, S. Gaba, T. Chang, X. Pan, W. Lu, *Nat. Commun.* **2012**, *3*, 732.

[17] Z. Xu, Y. Bando, W. Wang, X. Bai, D. Golberg, *ACS Nano* **2010**, *4*, 2515.

[18] I. Valov, E. Linn, S. Tappertzhofen, S. Schmelzer, J. van den Hurk, F. Lentz, R. Waser, *Nat. Commun.* **2013**, *4*, 1771.

[19] S. Peng, F. Zhuge, X. Chen, X. Zhu, B. Hu, L. Pan, B. Chen, R. Li, *Appl. Phys. Lett.* **2012**, *100*, 072 101.

[20] K. M. Kim, D. S. Jeong, C. S. Hwang, *Nanotechnology* **2011**, *22*, 254 002.

[21] S. M. Yu, H. S. P. Wong, *IEEE Trans. Electron Devices* **2011**, *58*, 1352.

[22] F. Mavré, R. K. Anand, D. R. Laws, K.-F. Chow, B.-Y. Chang, J. A. Crooks, R. M. Crooks, *Anal. Chem.* **2010**, *82*, 8766.

[23] G. Loget, J. Roche, E. Gianessi, L. Bouffier, A. Kuhn, *J. Am. Chem. Soc.* **2012**, *134*, 20 033.

[24] K. Peppler, C. Reitz, J. Janek, *Appl. Phys. Lett.* **2008**, *93*, 074 104.

[25] I. Valov, R. Waser, *Adv. Mater.* **2013**, *25*, 162.

[26] A. J. Bard, L. R. Faulkner, Electrochemical Methods: Fundamentals and Applications, Wiley, New York, USA **2000**.

[27] S. V. Kalinin, A. Borisevich, D. Fong, *ACS Nano* **2012**, *6*, 10 423.

[28] T. Nilges, S. Lange, M. Bawohl, J. M. Deckwart, M. Janssen, H. D. Wiemhofer, R. Decourt, B. Chevalier, J. Vannahme, H. Eckert, R. Weihrich, *Nat. Mater.* **2009**, *8*, 101.

[29] J. D. Slinker, J. A. DeFranco, M. J. Jaquith, W. R. Silveira, Y. W. Zhong, J. M. Mirabal, H. G. Craighead, H. D. Abruna, J. A. Marohn, G. G. Malliaras, *Nat. Mater.* **2007**, *6*, 894.

[30] W. M. Haynes, D. R. Lide, T. J. Bruno, CRC Handbook of Chemistry and Physics, 93rd ed. CRC Press, Boca Raton, FL, USA **2012**.

[31] R. Espiau de Lamaestre, H. Béa, H. Bernas, J. Belloni, J. L. Marignier, *Phys. Rev. B* **2007**, *76*, 20 5431.

[32] W. Leung, N. Cheung, A. R. Neureuther, *Appl. Phys. Lett.* **1985**, *46*, 543.